Viscoelastic properties of Red Blood Cells in a flow

Author: Marta Gironella Torrent.
Facultat de Física, Universitat de Barcelona, Diagonal 645, 08028 Barcelona, Spain.

Advisor: Fèlix Ritort.

Abstract: Red Blood Cells (RBC) are transported through blood stream and are responsible of oxygen delivery to the body tissues in vertebrates animals. This is achieved by squeezing RBC through body's capillaries, with mechanical properties being essential to achieve this function. Shape and composition of RBC are tightly related to their mechanical properties and their variation could induce several diseases and disorders. For that reason, the quantification of the mechanical properties of RBC could acts as an important biomarker. In this project we have performed flow experiments with RBC attached to a micron-sized bead using Optical Tweezers. The obtained results show two different populations of RBC characterized by the formation of a membrane microtube observed at high flow velocities values (800 μm/s or 50 pN of drag force). Analysing the force-velocity curves, we are able to differentiate these two populations and extract drag coefficient of RBC.

I. INTRODUCTION

Red Blood Cells (RBCs) are approximately a quarter of the total number of cells in the human body. Their structure and composition are optimized in order to carry out their main function, oxygen transport. In humans, the mature RBC lacks a nucleus allowing more room to store the oxygen-binding protein, haemoglobin, in this way increasing the transport capacity of oxygen. Moreover, the typical biconcave shape of RBCs increases their surface area facilitating the oxygen diffusion [1].

The main physiological RBC functions, as deformability and stability around the circulatory system, are related to their mechanical properties. The dysfunction of these mechanical properties is directly related with several diseases as sickle anaemia or malaria [2].

For that reason, the study of the mechanical properties of the RBC is of vital importance. Our approach to characterize them will be using single-cell methods. Single-cell techniques are experimentally challenging and grant access to physical quantities such as the force-velocity curve and the drag coefficient.

In order to achieve this aim we will use Optical Tweezers (OT) as our experimental device. We have chosen OT due to their accuracy and the fact they have been already successfully used for single-cell experiments with RBC [2–4].

II. MATERIALS AND METHODS

A. Experimetnal Setup

The optical trapping phenomenon consists in focalizing a laser beam using a microscope objective in order to push micron-sized dielectric particles due to the light radiation pressure (*Figure 1a*). These particles must have a refraction index higher than the surrounding medium to be pulled toward the focal point [5].

Our OT device uses two counterpropagating laser beams both focused in the same plane (*Figure 1b*). At this focal plane the two radiation pressures will be balanced, consequently, the dielectric particle will be trapped at the focal point [6].

The force range of OT reaches up to 100 pN, covering the range of forces involved in molecular and cell biology, hence it is an appropriate device to perform this kind of measurements [7].

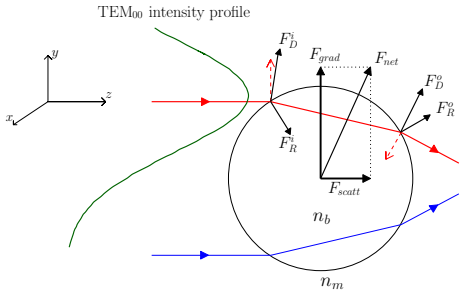

(a)Schematics of the principle of the light radiation pressure.

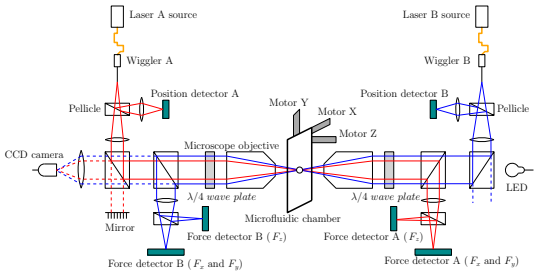

(b)Schematics of our optical tweezers.

FIG. 1: Basis of our experimental device.

The set of electronic devices which allows us to perform the experiments with OT are, according to the indexation of *Figure 2*:

1. *OT structure*: it is the main structure where we insert our michrofluidics chamber.

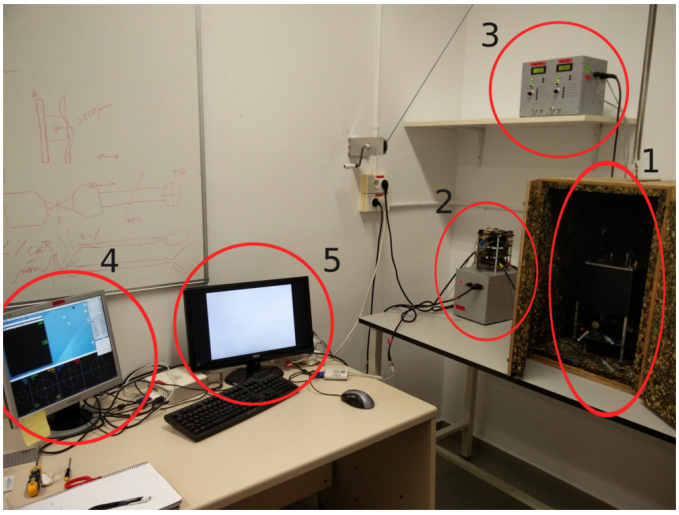

FIG. 2: Image of the electronic devices involved in the experiments.

2. *Electronic box and boards*: they communicate the PC with the OT structure.

3. *Laser power supply*: it controls the power of the lasers modulating the stiffness of the optical trap.

4. *PC with user interface program*: it allows us to modify the physical parameters of our experiments moving around our working zone.

5. *Real time CCD camera*: It gives us a real time video image of our working zone.

Our setup to carry out this type of experiments consists in a microfluidics chamber formed by three channels: the central and two lateral ones toward which we flow microbeads and RBC to the central channel through two dispenser tubes (*Figure 3*).

The microfluidics chamber used in these experiments is composed by two coverslips with a thickness around 150 μm and two pieces of nescofilm with channels shape and a thickness of 125 μm more or less. The central channel is 250 μm in thickness and 2 mm in height. The working zone is found in the middle of the central channel where the two lateral channel dispensers tubes are located.

We connect plastic tubes with syringes to the three channels in order to control our input. The output of our microfluidics chamber goes to a trash container.

A huge advantage of our microfluidics setup is the possibility of changing its design but, on the other hand, this fact decreases their reproducibility. Although all the microfluidics chambers are composed by the same elements, each of them are slightly different due to the fact that they are made by hand.

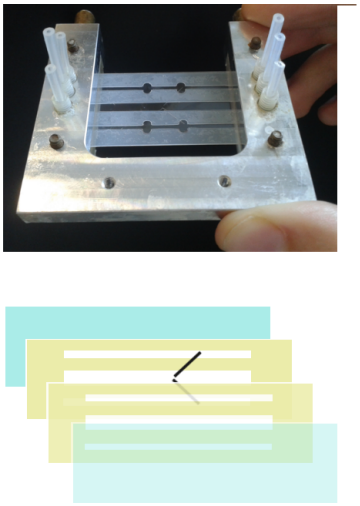

FIG. 3: Image and schematics of the micrhofluidics chamber. In the bottom the different components of the chamber: two coverslips, two nescofilm layers and two dispenser tubes.

B. RBC and Buffer preparation

Human RBCs were freshly prepared before each experiment by finger pricking of a healthy donor. Four microliters of blood were diluted in 1 mL of a PBS solution containing 130 mM NaCl, 20 mM K/Na phosphate buffer, 10 mM glucose, and 1 mg/mL BSA. RBCs were washed twice in the described PBS buffer by centrifugation (2 min, 200 g) and aspiration of the supernatant [3].

C. Micron-sized bead coated with fibronectin preparation

First we wash 1 ml (50 mg/ml) of microbeads 2x in 10 ml of water. After a second wash, we resuspend the pellet in 10 ml of PBS and we transfer it to the beaker. It is necessary to continuously stir the liquid to ensure that the microbeads are well suspended. While we mix it, we add 100 mg of EDC* with constant stirring. Then, we let react the mixture for 15 min at room temperature. After that, we wash again 2x in water, resuspend them in 5 ml of PBS and add fibronectin (saturation at approximately 400 ng/cm^2) to the solution. We let it react for 2-4 hrs at room temperature with constant stirring. At this point, we wash and resuspend our mixture in 4 ml of quenching solution ** and we gently mix the result for 30 minutes. The next step is to wash and resuspend the solution in storage buffer (5 ml) to the concentration of 10 mg/ml. Finally, we store it at 4°C (storage solution: BSA 0.1% in PBS).

*EDC=N-(3-Dimethylaminopropyl)-N'-ethylcarbodiimide hydrochloride (for example Sigma No. E6383).

** Quenching sol : 0.15 g glycine/50 ml water + 1 ml of 10% BSA.

III. EXPERIMENTAL REALIZATION

In the present project, we will perform RBC deformability studies by using optical tweezers assays to measure the drag coefficient of the RBC under different kind of mechanical stimuli. We will follow a global approach using Stokes force measurements. In order to perform our experiments easily, we will define 3 positions in the working zone: the two dispensers tubes where we will obtain microbeads (P1) and RBC (P2), and the position where we will fix our microbead-RBC system during the flow application (P3) which has to be properly determined (*Figure 4*).

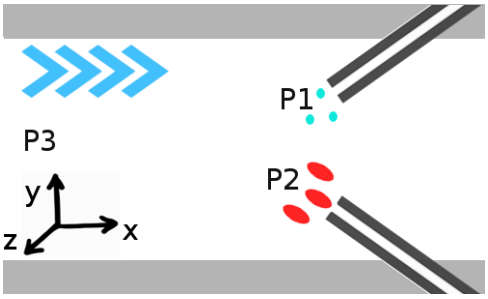

FIG. 4: Schematics of the three important positions of the working zone. The flow direction is indicated by the blue arrows.

Once we have prepared one eppendorf with RBC and another one with microbeads covered with fibronectin, we flow buffer in the three channels of our microfluidic chamber. First of all, we have to calibrate the force measurements in the microbead in the optical trap by aligning the lasers and focalizing them in the same focal plane. The calibration allows us to use the microbead as a dynamometer.

Then, we need to choose an appropriate position to perform our experiments, this position corresponds to P3 in *Figure 4*. In this proper position the hydrodynamic effects which could infer parasite contributions to our data have to be minimized. For a laminar flow which follows the Poiseuille law, as our buffer, this position will be located at the middle point of both Y and Z directions. The Y dimension of the central channel is huge compared with Z dimension (250 μm). For that reason, in Y direction, we approximately determine the middle point by computing the middle value of the distance between the two nescofilms. Once we get this point, we move there and we perform a Poiseuille flow test along the Z direction to accurately determine the final proper position.

In order to perform Poiseuille flow test, we immobilize a microbead with the optical trap and we apply a constant flow in the central channel connecting the syringe to an injection pump. Starting as close as possible to one of the coverslips we measure the force in the flow direction during 10 seconds. All the forces represented in our Figures are in the flow direction (X axis *Figure 4*) unless otherwise said. We repeat this procedure at several distances. The position where the force is maximum will be the Z middle point.

After determining the position where the experiments will be performed, we move to P1, flow some buffer with microbeads coated with fibronectin through the lateral channel and we trap one of them. Then, we move to P2 and flow some RBC from the other lateral channel.

If the RBC remains more than a few seconds in the same point where the trap is focused its membrane becomes damaged, and hence it is not a viable sample anymore. For that reason, as soon as we attach the microbead to a RBC it is necessary to move fast to P3 and apply a flow immediately (18 μL/min is the minimum flow for which the optical trap does not damage the RBC). Once we ensure that the RBC is not damaged we start our experiment. Starting from 18 μL/min we measure the force in the flow direction during 10 seconds, we increase the flow by 2 μL/min and we repeat the process until the microbead-RBC system detaches from the optical trap. After that, we move to P1 and we start the whole procedure again. In this way, we obtain different microbead-RBC force-flow experimental data.

Finally, in order to convert flow into velocity to compute the force-velocity curves, we perform Stokes measurements moving the chamber instead of applying a flow. This will allow us to control the velocity and measure the force to obtain the medium viscosity.

IV. DATA ANALYSIS

We will divide this section in four blocks: A) how are the force values with their corresponding statistical errors extracted from the force signals, B) how to determine the proper position where the experiments will be performed, C) how we get the medium viscosity, and finally, D) how to convert flow into velocity.

Knowing this information will allow us to compute force-velocity curves for multiple microbead-RBC systems from our non-treated experimental data of force signals associated with flow rates.

A. Analysis of force signals

The force signals that we recorded are Gaussian distributed (*Figure 5a*). Dividing the 10 seconds force signals in 5 signals of 2 seconds each one, we are able to compute a mean value and its corresponding statistical error for each original signal (*Figure 5b*).

We just have to compute the mean value with its standard deviation for the 2 seconds signals and apply the

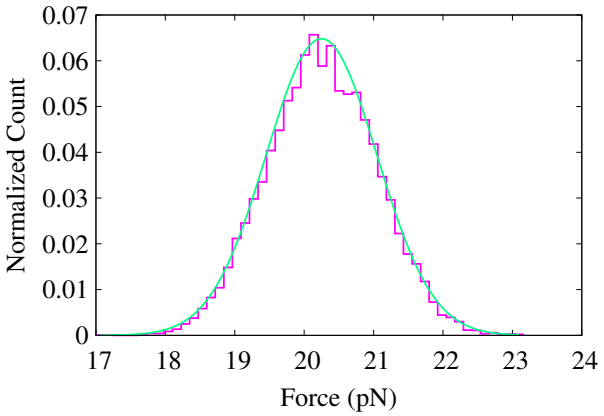

(a)Histogram of force obtained during a 10 seconds signal with a gaussian fit.

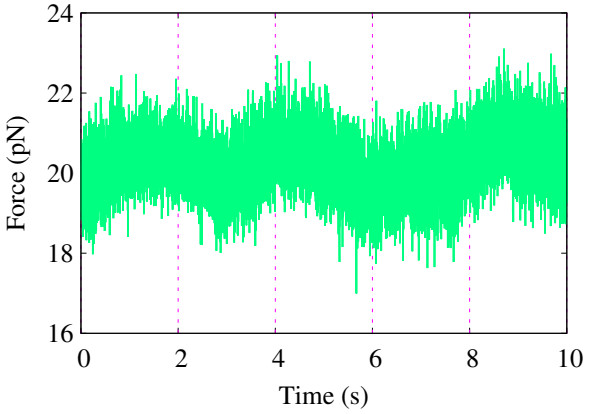

(b)Main signal of 10 seconds divided in 5 signals of 2 seconds. An oscillatory behaviour is observed due to the mechanical coupling with pump motor (*Appendix B*).

FIG. 5: Force signals analysis.

standard error expression which is given by:

$$Err = \frac{\sigma}{\sqrt{N}}\,,$$

where σ is the standard deviation and N is the number of segments in which we divided the original force signal.

B. Poiseuille test

In order to get the force profile to determine the proper position P3, we compute the mean value for each recorded signal as we explained in the previous section. We fit a parabola to the obtained data:

$$f(z) = Az^2 + Bz + C\,,$$

where $f(z)$ is force in the flow direction and z is the Z position.

The positions of the two coverslips will be the points where $f(z)$ becomes equal to zero so this gives us the width and the absolute scale for the Z direction. Consequently, we can identify the Z position where the maximum force is applied just putting to zero the first derivative $f'(z) = 2Az + B$. The proper Z position in terms of A and B parameters can be expressed as:

$$Z_{pos} = -\frac{B}{2A}$$

C. Stokes force measurements moving the chamber

The linear relation between force and velocity of an spherical object is given as:

$$F = 6\pi\eta R v\,,$$

where η is the viscosity of the surrounding medium and R the radius of the sphere. In the present case the sphere is a microbead.

The Stokes test moving the chamber provides us with a force signal for each velocity. Once we compute the values of force, velocity and their respective errors, we will be able to extract the drag coefficient of one microbead as the slope of its force-velocity curve. Finally, knowing a priori the microbead radius, it is possible to obtain the viscosity of the medium.

D. Stokes force measurements applying a flow

The aim of the Stokes flow measurements is the extraction of the force-velocity curve for each RBC. First of all, it is necessary to convert flow into velocity. In order to get that, we have measured the force signal of a single microbead applying flows from 18 μL/min to 48 μL/min.

Knowing the buffer viscosity we are able to transform force into velocity and get a velocity-flow curve. If we fit a linear relation to this curve as:

$$Velocity = \alpha FlowRate$$

we obtain the proportionality coefficient α. This will allow us to convert force-flow curves into force-velocity curves which gives us the quantitative information to characterize the global deformability of the RBC considering the microbead as a non-deformable object.

V. RESULTS

A. Poiseuille test

We have fitted our data to a parabola (*Figure 6*) and the parameters obtained are:

$$A = (-0.00149 \pm 0.00004)\ \mathrm{N}/\mu\mathrm{m}^2$$

$$B = (1.01 \pm 0.02)\ \mathrm{N}/\mu\mathrm{m}$$

$$C = (154 \pm 4)\ \mathrm{N}$$

so, making $f(z)$ equal to zero, we get that the relative positions of the two coverslips are $Z_1 = 232$ μm and $Z_2 = 446$ μm, and hence the width on Z direction has a value of $W_z = 214$ μm

In this particular microfluidics chamber the middle position along the Z direction is located at

$$Z_{pos} = (107 \pm 16)\ \mu\text{m}$$

away from both coverslips.

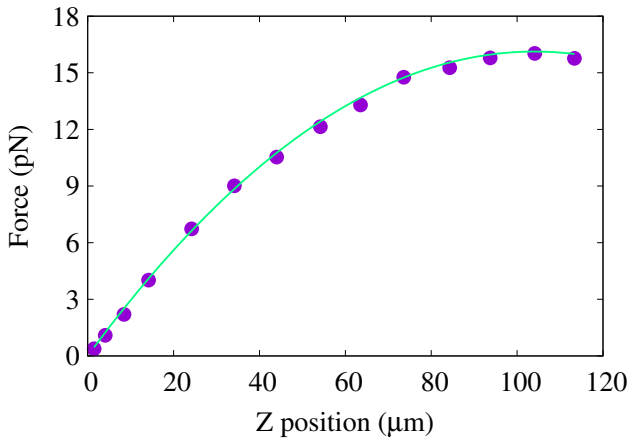

FIG. 6: Graphic representation of the force dependence with respect to the distance to one of the coverslips when a constant flow is applied. We consider that the coverslip is at $Z = 0$ μm.

B. Buffer viscosity

In order to extract the buffer viscosity we have done a linear fit to the force-velocity curve of a single microbead with a radius of (1.50 ± 0.01) μm (*Figure 7*). If we consider the microbead as an ideal spherical object of radius R, its drag coefficient γ is given by:

$$\gamma = 6\pi\eta R\,,$$

where η is the viscosity of the medium.

Imposing zero force at zero velocity we get the following drag coefficient

$$\gamma = (0.0262 \pm 0.0004)\ \text{pN·s}/\mu\text{m}$$

Finally, we obtain the viscosity of our buffer at 25°C applying the formula $\eta = \gamma/6\pi R$

$$\eta = (9.3 \pm 0.3)10^{-4}\ \text{Pa} \cdot \text{s}$$

which is slightly larger than the one of the water at the same temperature: $\eta = 8.910^{-4}$ Pa·s [8]. On the other hand, considering the errors, the viscosity of our buffer is compatible with the water one.

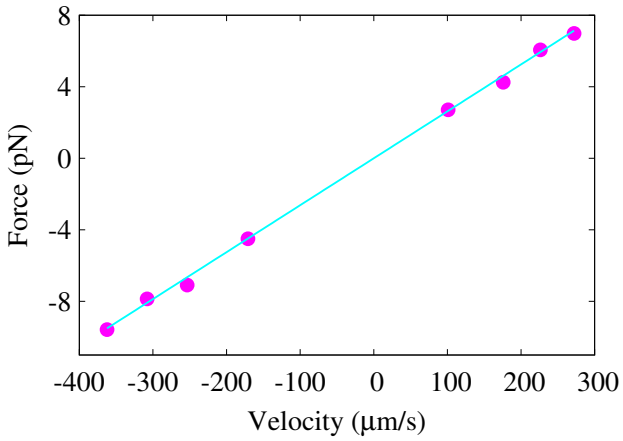

FIG. 7: Force-velocity curve of a calibration microbead (1.5 μm of radius).

C. Force-velocity curves

Knowing the radius of our microbeads and our buffer viscosity, we are able to convert force into velocity obtaining the linear relationship shown in *Figure 8*.

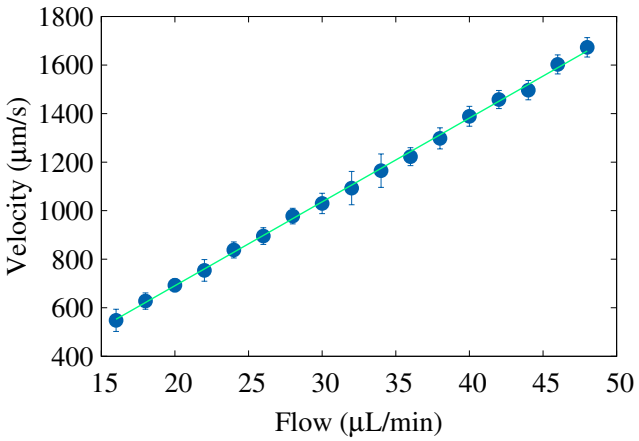

FIG. 8: Graphic representation of velocity against flow. We extract the proportionality coefficient between the two quantities by fitting a linear relation.

The result of the linear fit $V(Fr) = mFr$ where V is velocity and Fr is flow rate, is given by:

$$m = (34.5 \pm 0.1)\ \mu\text{m·min/s·}\mu\text{L}\ ,$$

where the units are inconsistent but coherent with our conversion due to the fact that the injection pump provides the flow rate in μL/min and we give the velocity in μm/s.

During the flow experiments, in some cases, the formation of a very thin membrane tube between the trapped microbead and the RBC was observed (*Figure 9*). For

vesicles it has already been reported and studied [4, 9–12]. This phenomenon occurs when the microbead-RBC system is subject to an applied force of approximately 50 pN (*Appendix C*). As a first hypothesis, we thought that this dynamic transition would be reflected in the force-velocity profile.

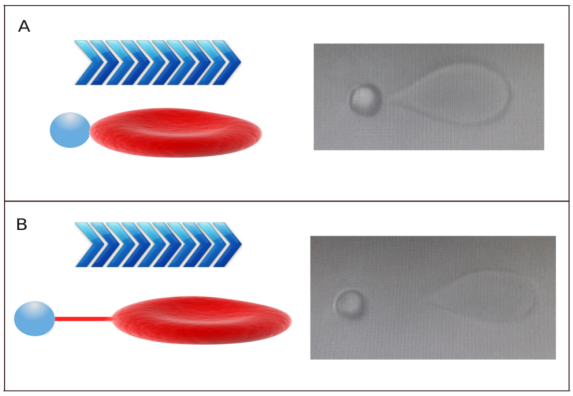

FIG. 9: A) Schematics and image of the population of RBC that does not present membrane microtube formation when we apply a flow. The RBC is bonded with a microbead fixed by the optical trap. B) Schematics and image of the population of RBC that presents membrane microtube formation when we apply a flow.

In *Figure 10* we present the force-velocity curves of 15 different microbead-RBC systems obtained by flow Stokes measurements.

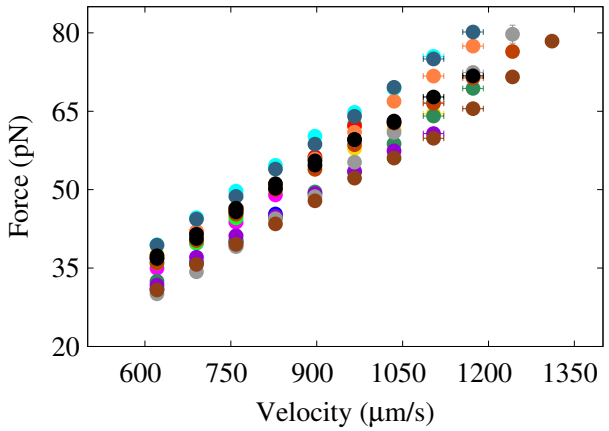

FIG. 10: Graphic representation of force versus velocity of microbead-RBC systems where the black curves represent the population without microtube formation. Each color represents a different microbead-RBC system.

Observing the curves individually, it is not obvious which of them correspond to which population, nor if they present a deviation from the linear behaviour. The RBC population which does not form microtube has a high reproducibility so we will average its force-velocity curves and take the result as the reference.

In order to observe if there are any differences between the two populations, we will compare the reference curve with each curve of the microtube population. To this end, we subtract the reference curve imposing that at 18 μL/min all the RBC are subject to the same force. Thus we obtain a residual force graphic showing the difference in behaviour between both populations (*Figure 11*).

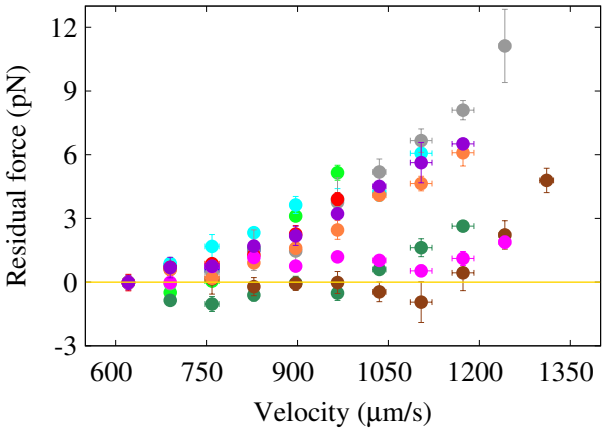

FIG. 11: Graphic representation of residual force against velocity for RBC which present microtube formation.

In order to obtain the RBC drag coefficient, as a first approximation, we can consider that the force contribution of the microbead is independent of the RBC one. This fact allows us to subtract the microbead contribution to the microbead-RBC force-velocity curve. Once we compute the isolated RBC curves, we are able to extract the drag coefficient of each RBC for every velocity value. Averaging all the drag coefficient values for each velocity, we obtain the dependence between these two quantities.

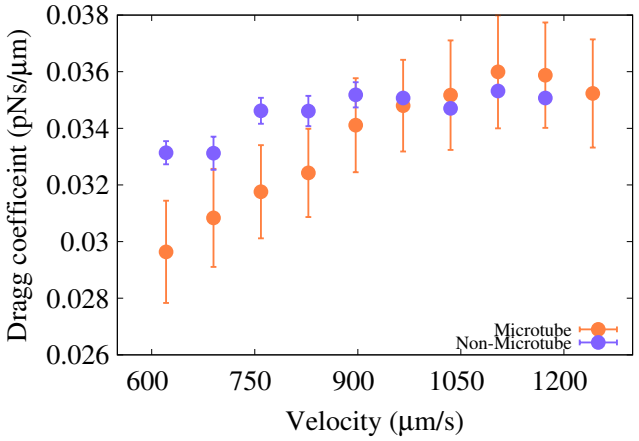

FIG. 12: Graphic representation of RBC drag coefficient against velocity for both microtube and non-microtube populations.

In *Figure 12* we observe that the population which does not form microtube presents a fairly constant drag coefficient. On the other hand, the behaviour of the microtube population seems to show two different regimes. The first one increases linearly until it reaches a maximum value while the second one remains constant at this maximum value that corresponds to the non-microtube population drag coefficient.

VI. CONCLUSIONS

Applying a flow to a trapped micron-sized bead attached to the RBC membrane allows us to measure the total drag force on the microbead-RBC system together with the global deformability of the RBC surface . In this kind of experiments we study the dependence of the total drag force against the velocity of the flow. For spherical objects (such as the micron-sized beads used in optical trapping experiments) Stokes law predicts a linear relationship between these two quantities, the slope being equal to the drag coefficient of the microbead. However for the microbead-RBC system there is no spherical symmetry and, in principle, such linear dependence would be lost for sufficiently large flow velocities. In fact, our experiments show the formation of a very thin filament connecting the RBC to the microbead around 50 pN of force. This behaviour is not shown by all the analysed RBC. There are some of them which do not present membrane microtube even at high velocities and remain attached to the micron-sized bead.

Comparing the force-velocity curves of these two populations, we are able to quantitatively characterize them and somehow differentiate which RBC present the formation of a membrane microtube. The microtube formation seems not to be related with RBC shape or size, in addition, the applied force for which microtube appears is no constant although it is around 50 pN. For that reason, the origin of these two populations could be due to a different RBC affinity to fibronectin or a non constant microbeads fibronectin concentration. The range in affinity or fibronectin concentration could explain the range of applied forces which the microtube is formed.

As a first approximation, we compute the drag coefficient of the RBC system considering the contributions of micron-sized bead and RBC as independent. We also quantitatively observe a difference between the microtube and non-microtube populations: the microtube population has an increasing drag coefficient that saturates at the value of the non-microtube one which is approximately constant.

Future work

We plan to change the injection pump for a pressure one in order to remove the mechanical coupling with the motor. This coupling is responsible of the oscillations in the force signal during the flow measurements and this fact does increase the error of the experimental results.

It could be very interesting to characterize the elongation of the membrane microtube in terms of the velocity flow using video image analysis. This methodology could be also used to quantify the recovery time of the microtube once we switch off the flow.

VII. APPENDIX

A. Comparison study of the two different injection pumps

There are two different injection pumps in our laboratory. Although we started with the simplest one, we realized that it was not precise enough for this kind of experiments due to the fact that the force signals obtained had a huge variance. At that point we performed a comparison study in order to determine if the other pump was more precise.

As a first step we compared the force distributions obtained with each pump (*Figure 13*). In this section pump 1 represents the simplest one which we used at the beginning and pump 2 the one which we have used to obtain all the data presented in this article.

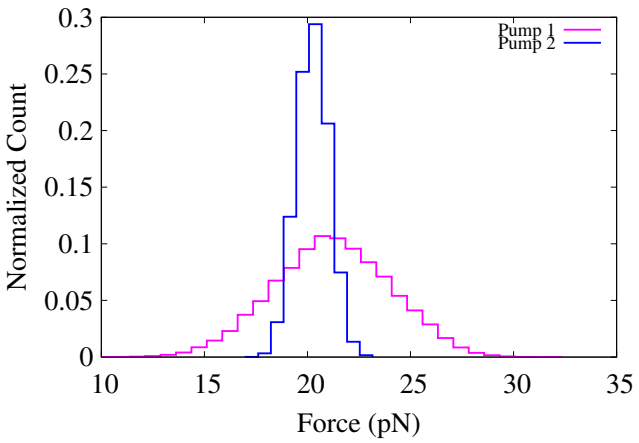

FIG. 13: Force distributions during a constant flow experiment for both pumps. As can be observed, pump 1 has a larger variance than pump 2 so the last one is more precise. Moreover, we observe that the mean values of the distributions are slightly different although we were applying the same flow rate. This might be due to the accuracy of pump 1.

Observing such a difference in the force distribution variance, we compared the standard deviation distributions obtained with the two different pumps. In order to get a standard deviation distribution, we performed flow Stokes measurements with a single micron-sized bead. In *Figure 14* we show that pump 1 induced a large error in force distributions while pump 2 induced a standard deviation around 1 pN.

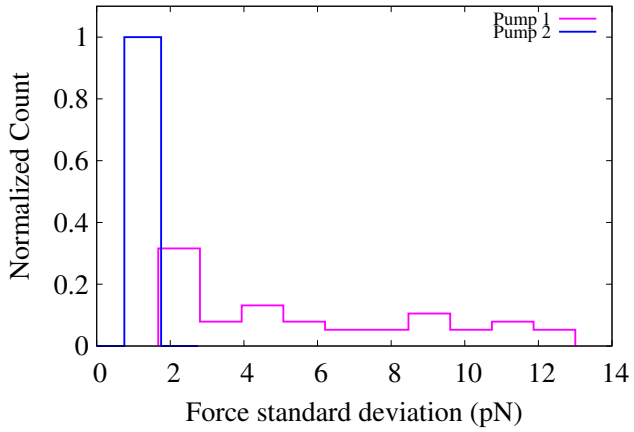

FIG. 14: Histogram of the standard deviation values of the force distributions for pump 1 and 2 obtained in flow Stokes measurements using a single microbead.

Taking into account that the minimum standard deviation that we could achieve is the one measured in pure diffusive experiments (0.5 pN), the 1 pN of pump 2 seems to be a good alternative. Nevertheless, we observe an oscillating behaviour in the force signal due to the pumping mechanism (*Figure 5* and *Appendix B*). This oscillation could induce an extra error. Moreover, it provides a non constant force in the microbead-RBC system during the measurements.

B. Mechanical coupling of injection pump 2

The experimental data presented in this study is taken using an injection pump which shows a mechanical coupling with the microfluidics setup. We observe this coupling in the force signal as an oscillating behaviour which can be characterized from the power spectrum analysis. Recording our measurements at high frequency we are able to compute the force power spectrum (FPS). A peak in FPS represents a sinusoidal contribution in the force signal.

In order to prove this mechanical coupling, we record high frequency force data when the central channel syringe is in contact with the pump but not connected. It means that the pump is working but in practise does not provide any flow.

At *Figure 15* we observe how the mechanical coupling induces a peak in the FPS. As a reference, we have measured the pure diffusion of a single microbead (0 μL/min) without any mechanical coupling from the injection pump. Then the peak is not observed.

In the case of pure diffusion, the FPS describes a Lorentzian shape given by the expression:

$$S(\nu) = \frac{k^2 K_B T}{2\pi^2 \gamma} \frac{1}{\nu_c^2 + \nu^2} ,$$

where ν_c is the corner frequency, k_B is the Boltzmann constant, T is the absolute temperature, and γ the drag coefficient affecting the trapped microbead [13].

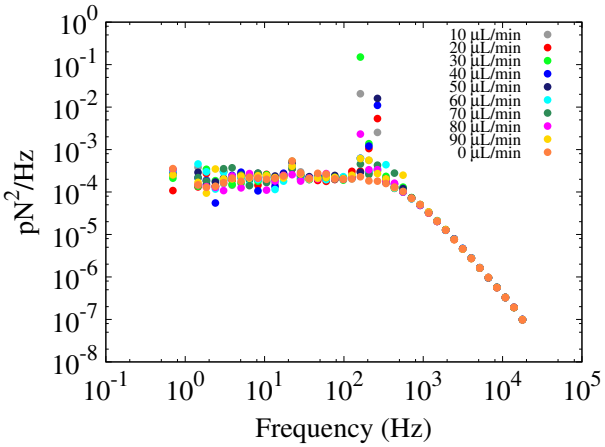

FIG. 15: Force power spectrum of a single microbead diffusion for different flow mechanical couplings.

C. Formation of membrane microtube movie

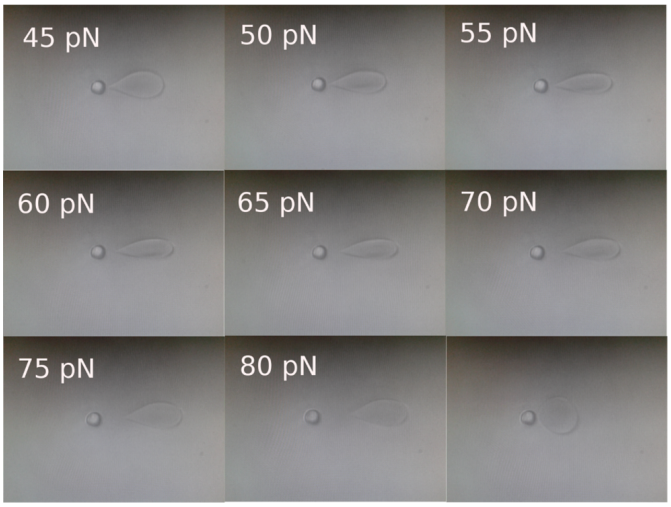

FIG. 16: Frames of the microbead-RBC system while the flow is increasing. The last frame shows how the RBC recovers if the flow is suddenly interrupted.

Acknowledgments

I would like to sincerely thank my advisor Fèlix Ritort for being balanced demanding and motivating pushing me to become a better researcher. I am deeply grateful to Marco Ribezzi for sharing his huge experience with me and help me to go ahead during the not easy moments of this project. I also would like to thank my colleagues of the Departament de Matèria Condensada, my friends from university, my professors, my flatmates and my family to be around during this intense year of work.

[1] L. Dean, *Blood Groups and Red Cell Antigens*, (NCBI, US 2005, 1st. ed.).

[2] Mauritz, Jakob MA, et al. "Biophotonic techniques for the study of malaria-infected red blood cells." *Medical & biological engineering & computing* 48.10 (2010): 1055-1063.

[3] Betz, Timo, et al. "ATP-dependent mechanics of red blood cells." *Proceedings of the National Academy of Sciences* 106.36 (2009): 15320-15325.

[4] Koster, Gerbrand, et al. "Membrane tube formation from giant vesicles by dynamic association of motor proteins." *Proceedings of the National Academy of Sciences* 100.26 (2003): 15583-15588.

[5] Ashkin, Arthur. "Acceleration and trapping of particles by radiation pressure." *Physical review letters* 24.4 (1970): 156.

[6] Smith, Steven B., Yuijia CUI, and Carlos Bustamante. "Optical-trap force transducer that operates by direct measurement of light momentum." *Methods in enzymology* 361 (2002): 134-162.

[7] Brouhard, Gary J., Henry T. Schek III, and Alan J. Hunt. "Advanced optical tweezers for the study of cellular and molecular biomechanics." *Biomedical Engineering, IEEE Transactions on* 50.1 (2003): 121-125.

[8] Kestin, Joseph, Mordechai Sokolov, and William A. Wakeham. "Viscosity of liquid water in the range -8°C to 150°C." *Journal of Physical and Chemical Reference Data* 7.3 (1978): 941-948.

[9] Rossier, O., et al. "Giant vesicles under flows: Extrusion and retraction of tubes." *Langmuir* 19.3 (2003): 575-584.

[10] Dasgupta, Raktim, and Rumiana Dimova. "Inward and outward membrane tubes pulled from giant vesicles." *Journal of Physics D: Applied Physics* 47.28 (2014): 282001.

[11] Waugh, RICHARD E. "Surface viscosity measurements from large bilayer vesicle tether formation. II. Experiments." *Biophysical journal* 38.1 (1982): 29.

[12] Bozic, Bojan, et al. "Shapes of nearly cylindrical, axisymmetric bilayer membranes." *The European Physical Journal E* 6.1 (2001): 91-98.

[13] Ribezzi-Crivellari, Marco, Anna Alemany, and Felix Ritort. "Universal axial fluctuations in optical tweezers." *Optics letters* 40.5 (2015): 800-803.